



Development of a three-dimensional geological model, based on Quaternary chronology, geological mapping, and geophysical investigation, of a watershed in the discontinuous permafrost zone near Umiujaq (Nunavik, Canada)

Richard Fortier^{1,2} · David-Roy Banville^{1,2} · Richard Lévesque³ · Jean-Michel Lemieux^{1,2} · John Molson^{1,2} · René Therrien^{1,2} · Michel Ouellet⁴

Received: 5 March 2019 / Accepted: 1 January 2020 / Published online: 27 February 2020
© Springer-Verlag GmbH Germany, part of Springer Nature 2020

Abstract

Among the few positive impacts of climate warming in cold regions, permafrost degradation can increase the availability of groundwater as a potential source of drinking water for northern communities. Near the Inuit community of Umiujaq in Nunavik, Canada, a watershed in a valley in the discontinuous permafrost zone was instrumented to monitor the impacts of climate change on permafrost and groundwater, and assess the groundwater availability and quality. Based on Quaternary chronology, knowledge of periglacial processes, and an investigation carried out in the valley (including mapping of Quaternary deposits and ice-rich permafrost distribution, drilling and sampling of deposits, and geophysical surveys), a three-dimensional (3D) geological model of the watershed was built into GoCAD to assess the hydrogeological context in this degrading permafrost environment. In total, six units were identified within the watershed including an upper aquifer in marine sediments, a lower aquifer at depth in glaciofluvial and glacial sediments, and the bedrock acting as a low-permeability boundary. An aquitard, made of frost-susceptible silty sand and discontinuously invaded by ice-rich permafrost, confines the lower aquifer. This 3D geological model clarifies the local stratigraphic architecture and geometries of Quaternary deposits, especially the stratigraphic relationship between the two aquifers, aquitard, and bedrock, and the extent of ice-rich permafrost within the watershed. It is the cornerstone to understand the groundwater dynamics within the watershed and to carry out numerical modelling of coupled groundwater flow and heat transfer processes to predict the impacts of climate change on groundwater resources in this degrading permafrost environment.

Keywords Quaternary deposits · Permafrost · Groundwater exploration · Geological model · Canada

This article is part of the topical collection “Hydrogeology of a cold-region watershed near Umiujaq (Nunavik, Canada)”

✉ Richard Fortier
richard.fortier@ggl.ulaval.ca

- ¹ Département de géologie et de génie géologique, Université Laval, Québec, Québec, Canada
- ² Centre d'études nordiques, Université Laval, Québec, Québec, Canada
- ³ Poly-Géo Inc., Saint-Lambert, Québec, Canada
- ⁴ Ministère de l'Environnement et de la Lutte contre les changements climatiques, Québec, Québec, Canada

Introduction

A reliable and safe source of drinking water is a critical component of northern communities for their sustainable development. Among the 14 Inuit communities in Nunavik (Québec), Canada, 12 rely on surface water as a supply of drinking water, while only two depend on groundwater (Lemieux et al. 2016). Although rivers and lakes are common in Nunavik, they are vulnerable to contamination, drying up, and freezing in winter. Groundwater is recognized to be a more secure and sustainable source of water but, being stored as ice in permafrost or located in deep aquifers, its availability is limited in cold regions. Nevertheless, as one of very few positive impacts of climate warming in cold regions, permafrost degradation can increase the availability of groundwater by releasing melt water in the ground and facilitating recharge

by surface-water infiltration through thawed layers which have become more permeable (Michel and van Everdingen 1994; Lemieux et al. 2016). The exploitation of groundwater resources to supply northern communities with drinking water in permafrost environments is therefore conceivable. The biggest challenge in such demanding environments is to identify aquifers with good groundwater productivity. The lack of relevant geological information in these environments and knowledge on Quaternary history and periglacial processes is a barrier for groundwater prospection in cold regions.

Numerical modelling of the impacts of climate warming on groundwater in degrading permafrost environments is a challenging task (Grenier et al. 2018). While significant insights on groundwater and permafrost dynamics were gained recently using parametric models (e.g. McKenzie and Voss 2013), a more in-depth understanding of their interaction and more accurate predictions can be obtained using realistic geological models (e.g. Walvoord et al. 2012). These models must be based on the Quaternary chronology and knowledge of the spatial extent of Quaternary deposits and permafrost environment in order to reflect the stratigraphic architecture and geometries of Quaternary deposits and permafrost, and be geologically reasonable (e.g. Ross et al. 2005). Geospatial information including digital elevation models (DEMs) and maps of Quaternary deposits, periglacial landforms, and drainage networks can constrain these models. Although naturally exposed cross-sections and very few borehole logs if available can provide ground truthing for local stratigraphy, defining the subsurface structures and ground conditions based only on surficial Quaternary geology and sparse boreholes and cross-sections is a major shortcoming. The use of complementary geophysical methods such as induced polarization tomography, ground penetrating radar profiling, seismic methods and electromagnetic surveys can overcome this problem by providing information on the bedrock topography (Légaré-Couture et al. 2018), extent of ice-rich permafrost (McClymont et al. 2013; Minsley et al. 2012), and the spatial distribution of aquifer and aquitard materials (Pugin et al. 2013). Three-dimensional (3D) geological mapping based on various field investigation methods is becoming increasingly popular for detailed hydrogeological studies (Thorleifson et al. 2010); however, there are few demonstrations of how to build them for cold-regions affected by permafrost.

The study presented herein is part of a strategic project to develop knowledge and expertise in cold regions hydrogeology for the sustainable use of groundwater in cold regions as a source of drinking water and for the sustainable management of this natural resource in the context of rapid socio-economic development, climate change, and permafrost degradation in northern regions. The central hypothesis of this project is that recent climate change is

having a major impact on groundwater dynamics in northern Quebec due to permafrost degradation. The current and anticipated permafrost degradation in Nunavik will likely increase the rate of groundwater recharge and lead to enhanced groundwater availability. In such a context, the groundwater resources can be used to supply drinking water to northern communities.

With the objectives to monitor and assess the impacts of climate warming on groundwater resources in a degrading permafrost environment, a small 2.23-km² watershed located in the Tasiapik Valley near the Inuit community of Umiujaq in the discontinuous but widespread permafrost zone in Nunavik (Québec), Canada, was identified and thoroughly studied. An integrated approach to assist groundwater exploration in cold regions, including cartography of surficial Quaternary geology, development of knowledge on Quaternary chronology and periglacial processes, and use of complementary geophysical methods to ensure a good spatial coverage of the watershed, was adopted to achieve this study. The results of geomorphological and geophysical investigations carried out in the watershed are presented herein, along with the development of a detailed 3D geological model of the watershed. This 3D geological model is the cornerstone of companion papers published as a topical collection in this issue of *Hydrogeology Journal*, to assess the hydraulic budget (Lemieux et al. 2020, this issue), groundwater geochemistry in the watershed (Cochand et al. 2020, this issue), groundwater flow in piezometers (Jamin et al. 2020, this issue), and to perform numerical modelling of coupled groundwater flow and heat transfer at the scale of permafrost mounds (Albers et al. 2020, this issue; Dagenais et al. 2020, this issue). A numerical groundwater flow model of the entire watershed based on this 3D geological model was also performed (Parhizkar et al. 2017). It is expected that the integrated approach used herein to delineate the cryo-hydrogeological context of the studied watershed in a degrading permafrost environment could serve as an example to identify groundwater resources in similar environments. Moreover, since there is a major knowledge gap with regard to groundwater availability in permafrost environments (e.g. Ireson et al. 2013), this detailed geological model will serve as a basis for quantifying groundwater exploitation potential along with evaluating aquifer sustainability in cold environments.

Study area

The study area is located in the discontinuous permafrost zone near the Inuit community of Umiujaq on the east coast of Hudson Bay in Nunavik (Québec), Canada, in a valley oriented north-west to south-east, informally named the

Tasiapik Valley (Figs. 1 and 2). More specifically, a small watershed within this valley was thoroughly studied. The watershed boundary and outlet in the Tasiapik Valley are identified in Fig. 3a.

The area covers a geologic contact between the Archean gneissic shield to the east and the overlying sedimentary and volcanic Paleoproterozoic sequences sloping gently towards Hudson Bay to the west. The landscape of the Umiujaq sector is characterized by cuestas with escarpments facing towards the east and dip slopes towards the west (Fig. 1). These cuestas were formed by erosion along lines of weakness in weakly inclined geological layers (KRG 2007). They culminate at elevations from 220 to 330 m relative to the current sea level north and south of the Tasiapik Valley, respectively. The cuesta dip slopes are composed of subaerial basalt lava flows which cover sequences of sedimentary rock. Both rock formations of the Nastapoka Group are visible along the cuesta escarpments (Fig. 2). The Tasiapik Valley is delimited to the north-east by the Umiujaq Hill, south-west by the cuesta escarpment, and south-east by Tasiujaq Lake, previously known under the names of Richmond Gulf or Guillaume-Delisle Lake (Figs. 1 and 2). The same rock formations which form the cuestas are visible along the slopes of the Umiujaq Hill. Tasiujaq Lake is a large body

of brackish water in contact with Hudson Bay through a narrow opening named Tursujuq, also known under the name *Le Goulet*, at the southwestern end of the lake. This lake lies in a graben of mid-Aphebian age (Chandler 1988) delimited to the west by the cuesta ridges.

Radiocarbon ages of the postglacial marine limit calibrated to take into account the variation in radiocarbon ^{14}C production rate over time show that deglaciation of the area took place around 8,000 calibrated years before present or 8,000 cal years BP (Lavoie et al. 2012). During the retreat of the Laurentide Ice Sheet (LIS), the land below the present elevation of about 250 m was submerged by the Tyrrell Sea (Allard and Seguin 1985). Glacio-isostatic rebound was first very fast at a rate of 60 mm/year, which then slowed down over the past thousand years reaching its current rate of 10 mm/year (Lavoie et al. 2012), but still remaining one of the fastest in the world. Following deglaciation of the area and under the combined effects of glacial retreat, marine transgression, isostatic uplift and steep topography, the depositional sequence of Quaternary sediments in the Tasiapik Valley is quite complex (Poly-Géo Inc. 2014) which leads to significant heterogeneity of the deposits. After emergence, these deposits were eroded, colonized by vegetation, and invaded by ice-rich permafrost (Allard and Seguin 1987).

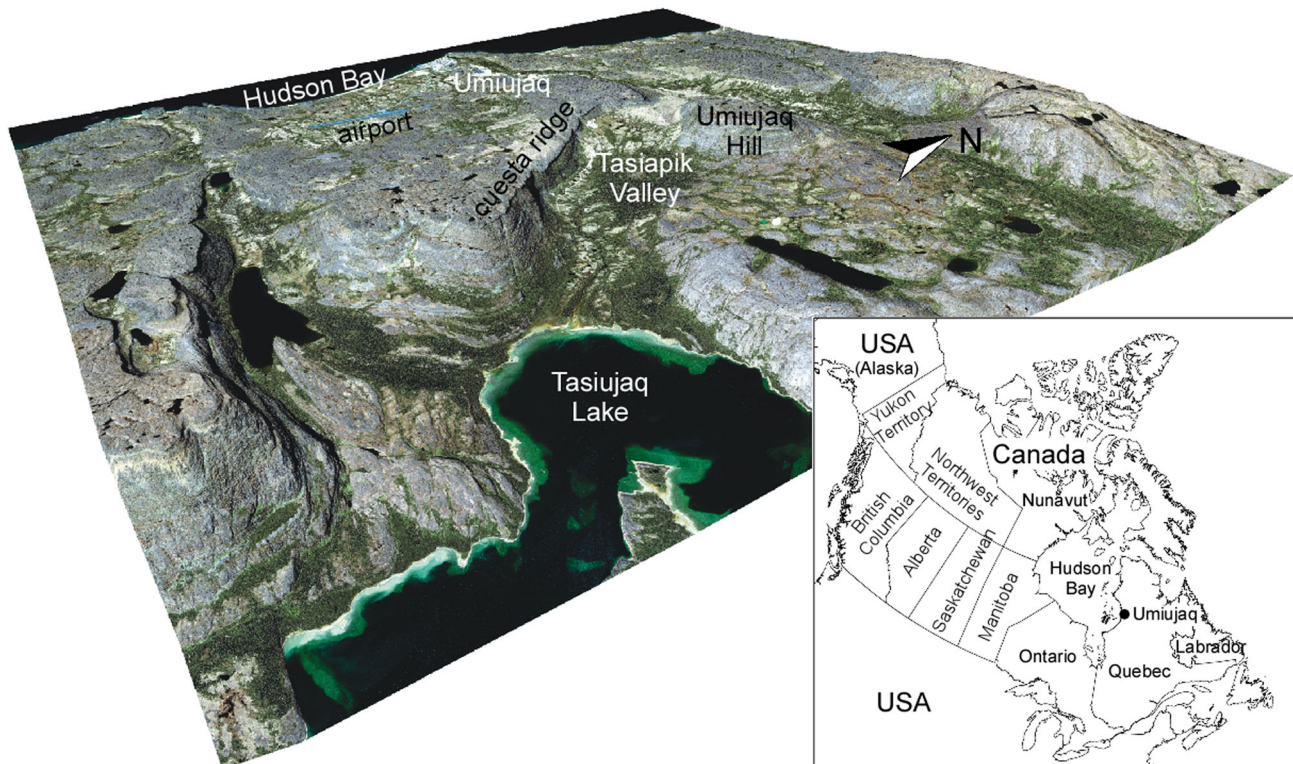


Fig. 1 IKONOS satellite image taken on July 27, 2005, draped on a digital elevation model of the region of Umiujaq along the east coast of Hudson Bay, Nunavik (Québec), Canada. West oblique view with artificial illumination from the south. Note the vertical exaggeration of

2:1. As a scale, the airstrip at the airport of Umiujaq is about 1.2 km long. Inset: map of Canada with the location of Umiujaq along the east coast of Hudson Bay

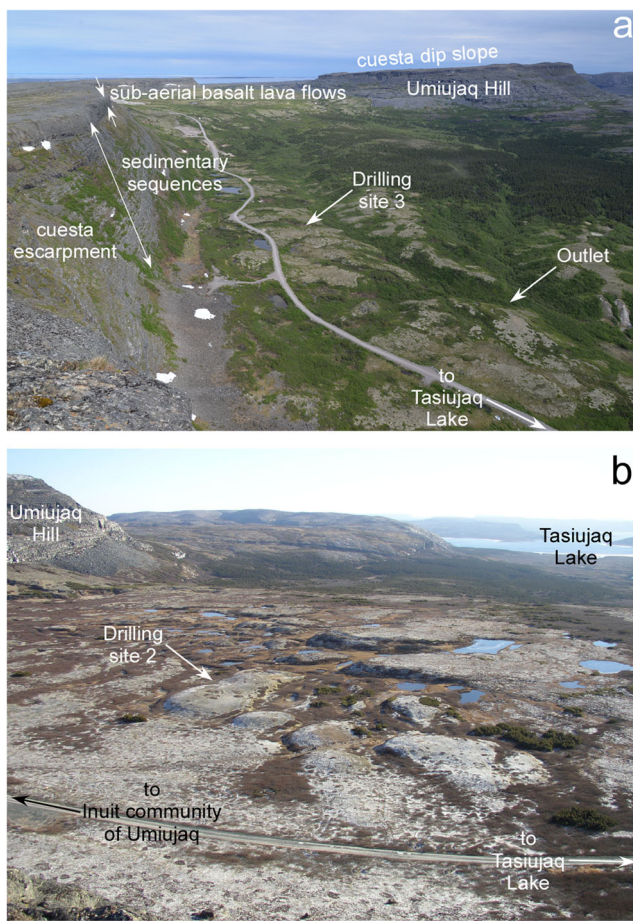


Fig. 2 Photographs of the Tasiapik Valley. **a** View toward the north of the valley. The grey zones in the foreground are ice-rich permafrost mounds. **b** View toward the south-east of the valley and Tasiujaq Lake. The dome-shaped forms in the foreground are ice-rich permafrost mounds. The gravel road leading to the Inuit community of Umiujaq and Tasiujaq Lake provides the scale. The drilling sites 2 and 3 are identified by arrows (see Fig. 3 for their location)

Numerous ice-rich periglacial features such as permafrost mounds sometimes called lithalsas (Allard et al. 1986) formed during the late Holocene in the frost-susceptible sediments deposited in valleys similar to the Tasiapik Valley (Allard and Seguin 1987). These permafrost mounds look like raised periglacial landforms (Fig. 2) due to the formation of segregation ice and subsequent frost heaving in the ground (Fig. 4).

Methods

The methods used to build the 3D geological model are spatial analysis of topography to delineate the watershed boundary, geological mapping, cross-sections descriptions, digging of shallow observation pits, borehole drilling for the installation of piezometers, paleo-reconstruction of the depositional

environment of Quaternary deposits, and geophysical investigation, which are described in the following subsections.

Watershed boundary

Thanks to a high-resolution digital elevation model (DEM) from an airborne laser detection and ranging (LiDAR) survey (Fig. 3b), the watershed boundary in the Tasiapik Valley was delimited by identifying the watershed outlet along a small stream and using spatial analysis tools in ArcGIS to define the heights of land (Fig. 3a).

Geological mapping

A map of Quaternary deposits and periglacial landforms in the Tasiapik Valley was constructed based on the interpretation of high-resolution color aerial photographs (Fig. 3a), the former DEM (Fig. 3b), and using on-site descriptions of exposed natural cross-sections and shallow observation pits for ground truthing. The final map of Quaternary deposits is shown in Fig. 3c.

Drilling campaign in the watershed

A network of 10 piezometers (Pz1–Pz10) and three thermistor cables (IMMATS1–IMMATS3) for monitoring hydraulic head and ground temperature, respectively, at 8 drilling sites not invaded by permafrost was installed during a drilling campaign in the watershed in summer 2012 (Fig. 3a). This network, called Immatsiak, which is part of the provincial network of groundwater monitoring wells of Québec (Government of Quebec 2019) aims to monitor the impacts of climate change on groundwater resources in a periglacial environment (Fortier et al. 2017). This network is completed by several automated thermistor cables in permafrost mounds, two meteorological stations including a rain-snow gauge, and a gauging station at the watershed outlet (for details, see Lemieux et al. 2020, this issue).

Examples of local stratigraphy observed at three drilling sites in the Tasiapik Valley are given in Fig. 5. Stratigraphic contacts as observed in each drilling site are also provided in the cryo-hydrogeological cross-section in Fig. 6b. The local stratigraphy is described in Table 1.

Geophysical investigation of the watershed

A geophysical investigation was performed along several geophysical survey lines in the Tasiapik Valley during the summers of 2011, 2013, and 2014 (Fig. 3b). The targets of this geophysical investigation were: (1) the layout of aquifer and aquitard materials within the studied watershed, (2) the bedrock topography as a low permeability boundary at depth, and (3) the horizontal and vertical extent of ice-rich permafrost.

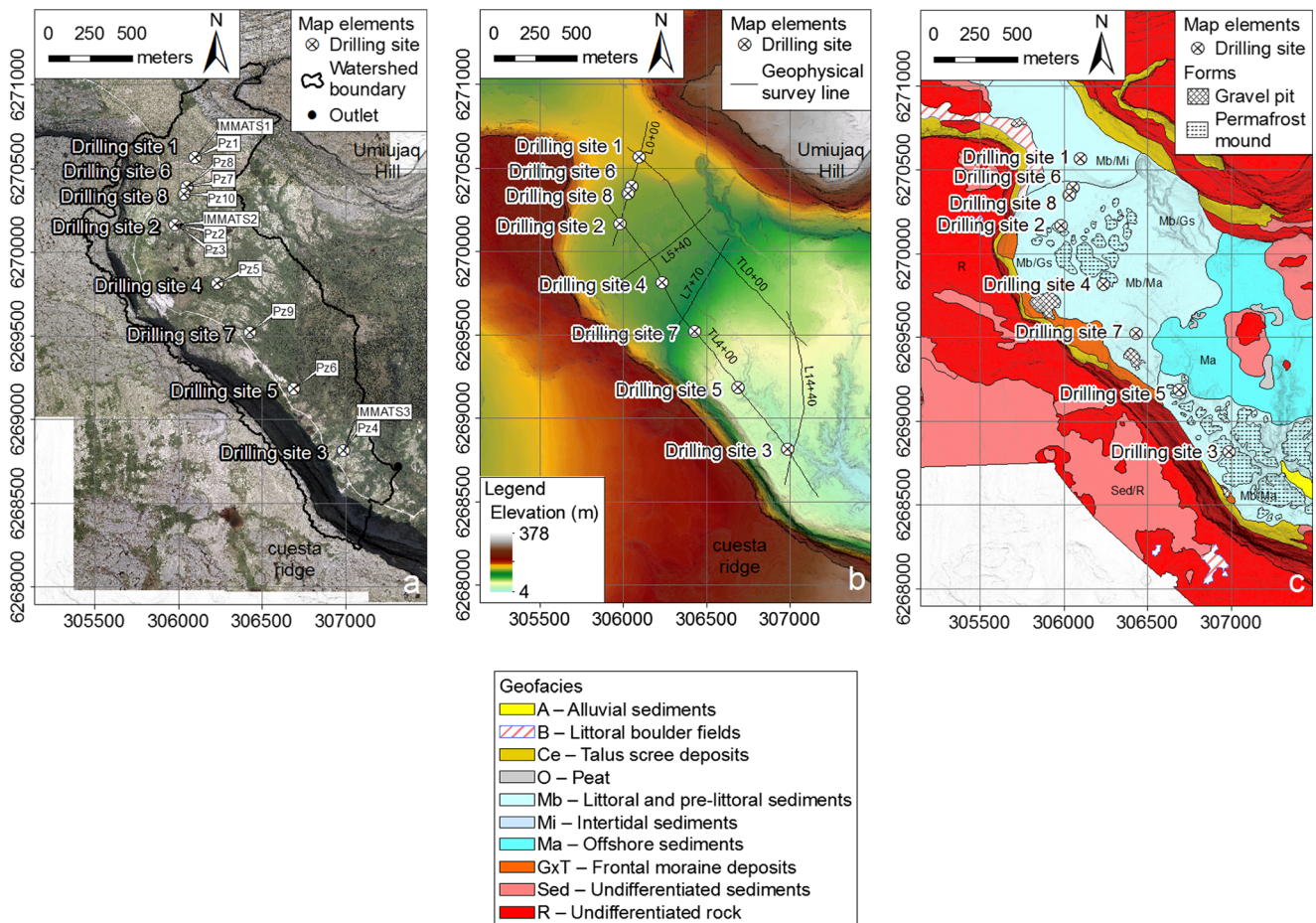


Fig. 3 Geospatial information available in the Tasiapik Valley, Umiujaq, Nunavik (Québec). **a** Mosaic of colour aerial photographs Nos. 031, 033, 035, 049, 051, 053, 077, 079, and 081 from the series Q10801 at a resolution of 15 cm taken on August 22, 2010 (all rights reserved to the Ministère de l’Énergie et des Ressources naturelles du Québec). The drilling sites, the groundwater monitoring wells, and the meteorological

stations of the Immatsiak network are identified on this map. **b** Digital elevation model from an airborne LiDAR (laser detection and ranging) survey carried out on August 22, 2010. In addition to the drilling sites, the geophysical survey lines are also identified on this map. **c** Map of Quaternary deposits (modified from Poly-Géo Inc. 2011 and 2014)

The geophysical methods used for this investigation are induced polarization tomography (IPT), ground penetrating radar (GPR) profiling, and seismic refraction tomography (SRT); IPT and GPR are complementary geophysical methods (De Pascale et al. 2008). On one hand, while the GPR profile provides stratigraphic information at high resolution, the soil layers cannot be identified a priori. On the other hand, ground conditions can be assessed from the IPT; however, the stratigraphic contacts cannot be accurately located in the models of electrical resistivity and chargeability found from the inversion of IPT since these models are characterized by smooth contrasts of electrical resistivity and chargeability, while sharp contrasts are expected at the corresponding stratigraphic contacts. SRT is useful for validating the interpretations of IPT for deep contacts such as the bedrock contact. The combined interpretation of the IPT, GPR, and SRT surveys can provide a detailed cross-section along the same geophysical survey line.

The IPT surveys were carried out using a dipole–dipole array with a fixed dipole length (a) of 20 m and 8 separations. Readings were taken every 10 m along the survey lines using a 2000 W TxII Transmitter to inject high electrical currents between 0.1 and 1 A and a GRx8-32 Receiver from Instrumentation GDD Inc. Both apparent electrical resistivity and chargeability were recorded with this receiver. Current waveform had 2 s on time with alternating polarity and 2 s off time. Decay curves of electrical potential in absence of electrical current from the transmitter were sampled using 20 gates of 80 ms each to assess the electrical chargeability. An example of electrical resistivity and chargeability models developed from the inversion of IPTs carried out along the geophysical survey lines L0 + 00 and TL4 + 00 is given in Fig. 6a (see Fig. 3b for the location of survey lines). These two survey lines which have been combined in a single section intersect all eight drilling sites (Fig. 3b). The spatial coverage of IPTs

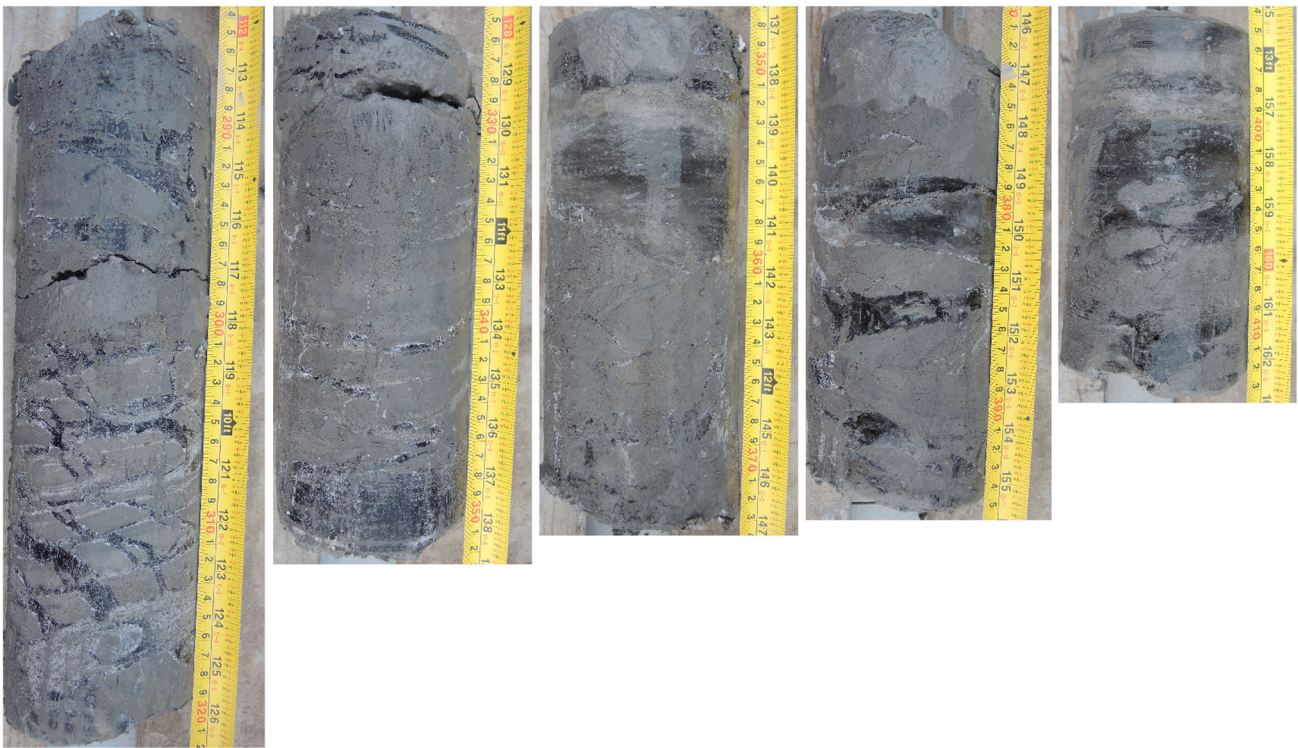


Fig. 4 Ice-rich permafrost samples (cryofacies Pmf) in frost-susceptible silty sand of the geofacies Ma (Table 1). The subhorizontal ice lenses appear as dark layers in these photographs. Thin subhorizontal light grey

sandy layers are also visible. The yellow measuring tape with centimetre and inch rulers provides the scale

along survey lines in the watershed (Fig. 3b) is shown in Fig. 7 in the form of fence diagrams of electrical resistivity and chargeability models. The software RES2DINV from Geotomo Software was used to perform the inversion of IPT data (Loke 2004).

The GPR profiles were performed using a pulseEKKO PRO from Sensors & Software Inc. and antennas at a nominal frequency of 100 MHz separated of 1 m. The antennas were mounted on a cart with a wheel odometer to control the data acquisition at a distance interval of 0.2 m. A GPS receiver was integrated to the cart for localising the GPR profiles along the survey lines. A time window of 900 ns to reach a depth of investigation in excess of 40 m and a time interval of 0.8 ns were used to digitalize the electromagnetic signal of each trace measured at the receiver antenna. In addition to the common-offset reflection configuration to achieve the GPR profiles, several common mid-point (CMP) surveys were carried out to assess the velocity of electromagnetic signal propagating in the ground. An example of a GPR profile along the geophysical survey line L0 + 00 is provided in Fig. 8.

The SRT surveys were carried out using a master seismograph StrataVisor NZ 24 interfaced with a slave seismograph 24-channel Geode manufactured by Geometrics Inc. for a total of 48 geophones. The distance interval was 5 m between the geophones and 15 m between the seismic shots. Each seismic shot was located

between two geophones. The impacts of a sledge hammer of 10 kg on a metal plate resting on the ground were used as a seismic source. The location and elevation of each geophone and seismic shot were measured with a differential GPS system. The velocity models developed from the inversion of SRT surveys are not provided herein (see Banville 2016).

Three-dimensional geological modelling of the watershed

A detailed descriptive approach to define the extent of Quaternary deposits and ice-rich permafrost in the Tasiapik Valley in a 3D geological model is challenging due to the complexity of the local stratigraphy (Table 1), the heterogeneity of the deposits, and the gradual transition between the different geofacies observed in the valley. A genetic approach would require a detailed description of the stratigraphy observed in several deep boreholes and along several stratigraphic sections, and using a dense coverage of geophysical survey lines which would have been too much expensive. This approach also requires a good knowledge of the Quaternary history, deposition processes taking place within the studied watershed, and spatio-temporal links between the geofacies observed in the watershed.

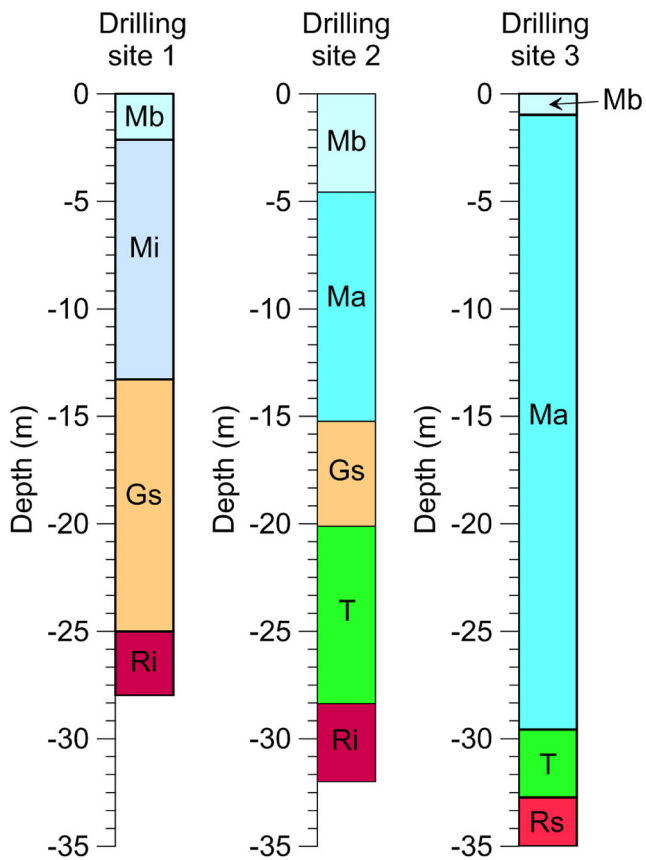


Fig. 5 Stratigraphic columns at drilling sites 1, 2, and 3. See Fig. 3 for the location of the drilling sites in the Tasiapik Valley and the legend (geofacies: Gs subaqueous outwash sediments; T till; Ri igneous rock; Rs sedimentary rock)

However, such a description is not needed for understanding groundwater dynamics and for numerical modelling of groundwater flow and heat transfer in the watershed to predict the impacts of climate warming on groundwater in this degrading permafrost environment. Only the different types of material in the watershed which control their physical properties such as the hydraulic conductivity, thermal conductivity, and geophysical properties, and the spatial extent of their stratigraphic contacts are needed to achieve a comprehensive geological model of the studied watershed. However, it is fundamental to take into account the genesis of observed geofacies and their stratigraphic relationships for establishing descriptive criteria to discriminate from these geofacies a small number of units in this geological model (Table 1).

All available data including the geospatial information (Fig. 3), the borehole logs (Figs. 5 and 6b), and the results from the geophysical investigation (Figs. 6, 7, and 8), along with other sources of information including cone penetration tests and other geophysical investigations (Buteau et al. 2005; El Baroudi and Fortier

2014; Fortier et al. 2008; Fortier and Yu 2012; LeBlanc et al. 2004; LeBlanc et al. 2006), were used to build a 3D geological model of the studied watershed in the Tasiapik Valley (Fig. 9). This model appears not only in the form of 3D surfaces delineating the contacts between the different units (Fig. 9) as identified in Table 1 but also in the form of maps of unit thickness (Fig. 10). Moreover, the floating volumes of ice-rich permafrost appear in Fig. 9h while the extent and estimated volume of permafrost mounds are provided in Fig. 10f.

The 3D surfaces of the geological model were constructed in GoCAD using the method of discrete smooth interpolation or DSI (Mallet 1992). A surface can be modelled with the DSI method taking into account certain geometric constraints while optimizing its smooth appearance (Mallet 1992). In the absence of constraints, such as stratigraphic contacts identified in boreholes, the DSI method tends to retain the original shape of the initial surface. The initial surfaces modelled by the user are therefore of great importance where there are no constraints. The user's knowledge on Quaternary chronology, depositional processes, stratigraphic relationships between units, and stratigraphic architecture and geometries expected for the units is critical in modelling the initial surfaces. In total, four 3D surfaces composed of triangular pixels were modelled to separate the five units (Table 1): (1) the bedrock surface (unit R), (2) the undifferentiated gravelly sand surface (unit T), (3) the medium sand surface (unit Gs), and (4) the silty sand surface (unit Ma; Fig. 9c–f). Each surface represents the upper limit of a given unit or the interface with the units above it. A last surface is the model surface from the DEM (Figs. 3b and 9g).

Three types of constraint were used to construct these four 3D surfaces: (1) control nodes, (2) border constraints, and (3) control points. The control nodes were robust constraints from the available ground truth information such as stratigraphic contacts observed in boreholes. To respect such a constraint, the mesh size of the surface was modified so that a node which is a vertex common of three triangular pixels corresponded exactly to this constraint. Border constraints only applied to nodes located at the edge of a surface such as unit boundaries outcropping at the surface (Fig. 3c). Control points were used as soft constraints to guide the discrete smooth interpolation using interpretative information derived from the geophysical investigation. Using the DSI method, the gaps between the modelled surface and control points were minimized while maintaining a smooth appearance of the surface.

Since the deep units influence the modelling of units closer to the surface, the first surface to be modelled was the bedrock. The four surfaces were constructed in three

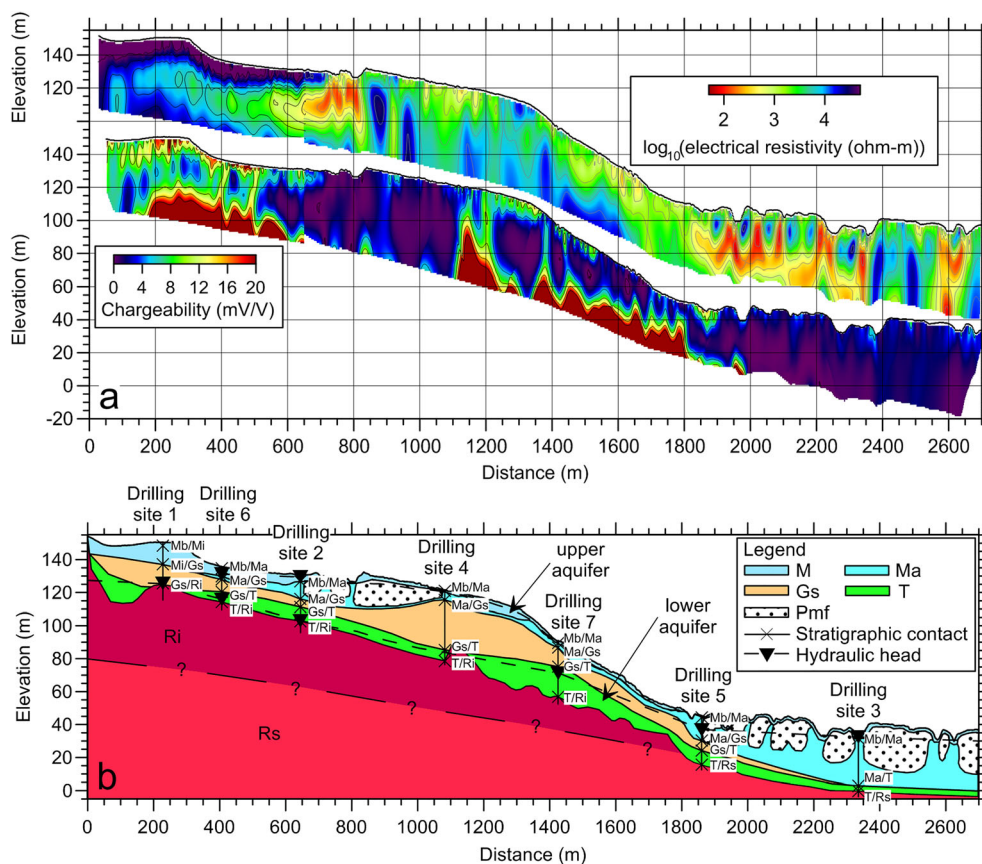


Fig. 6 **a** Merged models of electrical resistivity and chargeability obtained from the inversion of IPT surveys performed along the geophysical survey lines L0+00 and TL4+00 in the Tasiapik Valley. **b** Interpretative cryo-hydrogeological cross-section assessed from these models and the synthesis of geospatial information (Fig. 3) and

stratigraphic logs (Fig. 5). The stratigraphic contacts are identified along the boreholes at the drilling sites. See Fig. 3b for the location of the geophysical survey lines and drilling sites, and Table 1 for the legend of geofacies and units. Note the vertical exaggeration of 5:1 for these models and cross-section

steps: (1) a first draft of the geological model was built using all available information, (2) the surfaces were modified following a comparison between the synthetic cross-sections found by probing the first draft of the geological model at the location of the geophysical survey lines and the interpretative cross-sections obtained from the geophysical investigation (e.g. Fig. 6b), and (3) the maps of unit thickness to assess the spatial extent of the units were analysed for any inconsistency. The thickness of each unit in the Tasiapik Valley was assessed and mapped (Fig. 10) from the 3D surfaces delineating the contact between the different units of the geological model (Fig. 9). The modifications to the model to improve agreement with the results of the geophysical investigation were based mainly on qualitative comparisons which did not allow the development of other

quantitative constraints to help in modelling the surface. These modifications were therefore interpretative.

Results

Depositional environment in the Tasiapik Valley

As shown in the map of Quaternary deposits (Fig. 3a), a complex patchwork of glacial, glaciofluvial, marine, and alluvial sediments, which is closely related to the chronosequence of deglaciation and subsequent marine episode, is found in the valley bottom. The geofacies of unconsolidated sediments in addition to a cryological geofacies found in the Tasiapik Valley (Table 1) are described herein focusing on their

Table 1 Stratigraphy of the Tasiapik Valley

Epoch	Geofacies ^{a,b}	Formation	Lithology (hydrostratigraphic unit)	Unit (material)
Holocene	Mb $D_{10} = 0.216$ mm	Littoral and pre-littoral sediments	Sand and gravelly sand reworked by wave action (upper aquifer above the Ma geofacies)	M (undifferentiated sand)
	Mi $D_{10} = 0.160$ mm	Intertidal sediments	Inclined beds of sand transported by currents in the opening in the proto Tasiujaq Lake between the cuesta escarpment and the Umiujaq Hill (upper aquifer above the Ma geofacies)	
	Ma (cryofacies Pmf) $D_{10} = 0.008$ mm	Offshore sediments	Sandy silt and silty sand deposited in the Proto Tasiujaq Lake (Tyrrell Sea) and discontinuously invaded by permafrost (aquitard)	Ma (silty sand) Pmf (ice-rich permafrost)
	Gs $D_{10} = 0.110$ mm	Subaqueous outwash sediments	Medium sand deposited at the mouth of subglacial tunnels entering the proto Tasiujaq Lake (Tyrrell Sea) (lower aquifer partially confined by the Ma geofacies invaded by permafrost)	Gs (medium sand)
	GxT	Glaciofluvial sediments (frontal moraines)	Sand and gravel with blocks and fine-grained matrix deposited along the cuesta front (traces of shells)	T (undifferentiated gravelly sand)
	T $D_{10} = 0.326$ mm	Glacial sediments (till or diamicton)	Sand and gravel deposited by the ice sheet forming a continuous blanket in the valley bottom (lower aquifer partially confined by the Ma geofacies invaded by permafrost)	
Paleoproterozoic	Ri	Igneous bedrock	Hematized basalt – Persillon Formation, Richmond Gulf Group (fractured aquifer with low productivity)	R (undifferentiated bedrock)
	Rs	Sedimentary bedrock	Arenite – Pachi Formation, Richmond Gulf Group (fractured aquifer with low productivity)	

^a As proposed by Parent et al. (2010)

^b D_{10} is the effective diameter corresponding to 10% finer in the particle-size distribution

chronology of deposition, structural features, and stratigraphic relationships with other geofacies.

Depositional chronology of Quaternary deposits

The depositional sequence of Quaternary deposits in the Tasiapik Valley is closely related to the marine transgression and glacio-isostatic rebound in the area of Umiujaq. At the beginning of deglaciation in the area of Tasiujaq Lake around 8,200 cal years BP (Lavoie et al. 2012), the elevation of the relative postglacial sea level was about 250 m. Since deglaciation until land emersion in the lower part of Tasiapik Valley around 2,000 cal years BP, the physical processes of sedimentation of particles in suspension, resedimentation due submarine landslides and traction current, littoral reworking action, and erosion (Eyles et al. 1985) at the origin of the Quaternary deposits in the valley were active.

Glacial sediments (geofacies T)

Before deglaciation, a discontinuous till veneer made of coarse-grained materials (geofacies T) on the bedrock was left in the valley bottom by the LIS (Figs. 5 and 6b). The till thickness

varies from 5 to 10 m and is made of coarse-grained materials. No fine particles were observed in the till samples from the drilling. This absence of fine particles may be due to the circulation of drilling fluid used to wash out the drilling cuttings; however, any fine particles in the till could also have been washed out by the large influx of meltwater in subglacial streams during LIS retreat. In such conditions, the till would have been reworked. This geofacies is a very good granular aquifer.

Glaciofluvial sediments (geofacies GxT and Gs)

During deglaciation from about 8,200 to 8,000 cal years BP (Lavoie et al. 2012), frontal moraines were deposited along the cuesta escarpment and at the toe of the Umiujaq Hill (geofacies GxT; Fig. 3c). Moreover, near the ice front of the retreating LIS, large masses of sediments were ejected by strong subglacial meltwater streams (geofacies Gs; Figs. 5 and 6b). These conditions are characteristic of submarine fans near ice fronts (Lønne 1995). This subaqueous outwash unit is made of sand and gravel, and can be as thick as 30 m. While this unit is also a very good granular aquifer, it is absent downstream in the watershed (Figs. 5 and 6b).

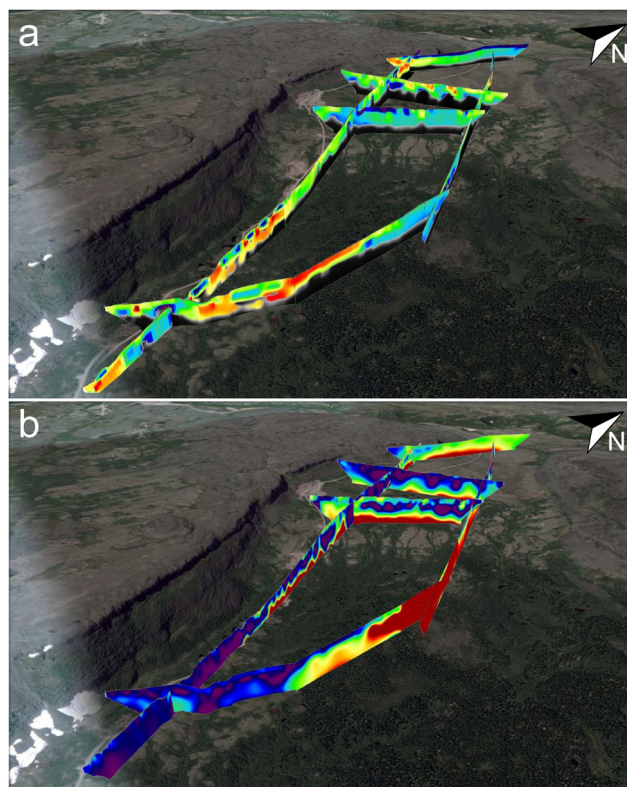


Fig. 7 Geophysical investigation coverage in the Tasiapik Valley (see Fig. 3b for the identification and location of the geophysical survey lines). Fence diagrams of models of electrical resistivity (Fig. 7a) and chargeability (Fig. 7b) superimposed on a Google satellite image draped over a digital elevation model of the Tasiapik Valley. The color scales are the same as in Fig. 6a. There is no vertical exaggeration in this view

Offshore sediments (geofacies Ma)

Fine-grained marine materials (geofacies Ma made of silty sand) started to deposit in calm water around

7,500 cal years BP as soon as the ice front retreated from the valley. Since the water column was higher in the lower reaches of the valley (about 150 m) compared to the upper valley (about 50 m), the thickness of the geofacies Ma is relatively greater in the lower valley, where it is up to 25 m (Figs. 5 and 6b). This geofacies was absent at drilling site 1 but was sampled at the other drilling sites including drilling site 6, being the closest to drilling site 1 (Figs. 5 and 6b). The sedimentation conditions in the upper valley with a thin water column and active current traction were not favorable for the formation of this geofacies, which first appears close to drilling site 6 (Fig. 6b). Following erosion of the littoral and pre-littoral unit—geofacies Mb; see section ‘Littoral and pre-littoral sediments (geofacies Mb)’—by fluvial action, this offshore unit outcrops in the lower part of the valley (Fig. 6b).

Intertidal sediments (geofacies Mi)

Before the beginning of emergence of the Quaternary deposits at the head of Tasiapik Valley around 6,875 cal years BP, between the cuesta front and Umiujaq Hill which remained above sea level following the marine transgression, the upper valley was an opening of the proto Tasiujaq Lake into Hudson Bay, similar to the only existing opening—namely the Tursujuq opening. During rising tides, the tidal currents in this opening and the rushing sea water of Hudson Bay into the proto Tasiujaq Lake had enough energy to transport sandy materials which were deposited to form a thick sand cover above the geofacies T and Gs in the upper reaches of the Tasiapik Valley (Fig. 8). This geofacies Mi is characterized by beddings inclined to the south

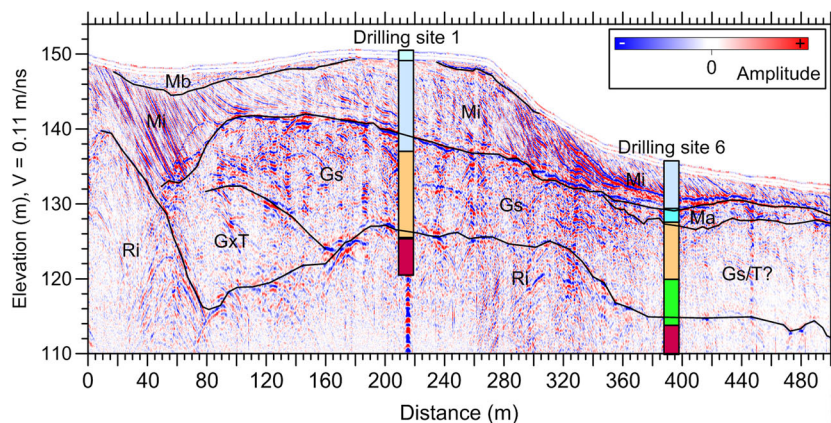


Fig. 8 GPR profile along the geophysical survey line L0+00 in the Tasiapik Valley. The interpretative cross-section and stratigraphic columns at drilling sites 1 and 6 are superimposed on the GPR profile. See

Fig. 3b for the location of the geophysical survey line and drilling sites 1 and 6, and see Table 1 for the legend. Note the vertical exaggeration of 5:1

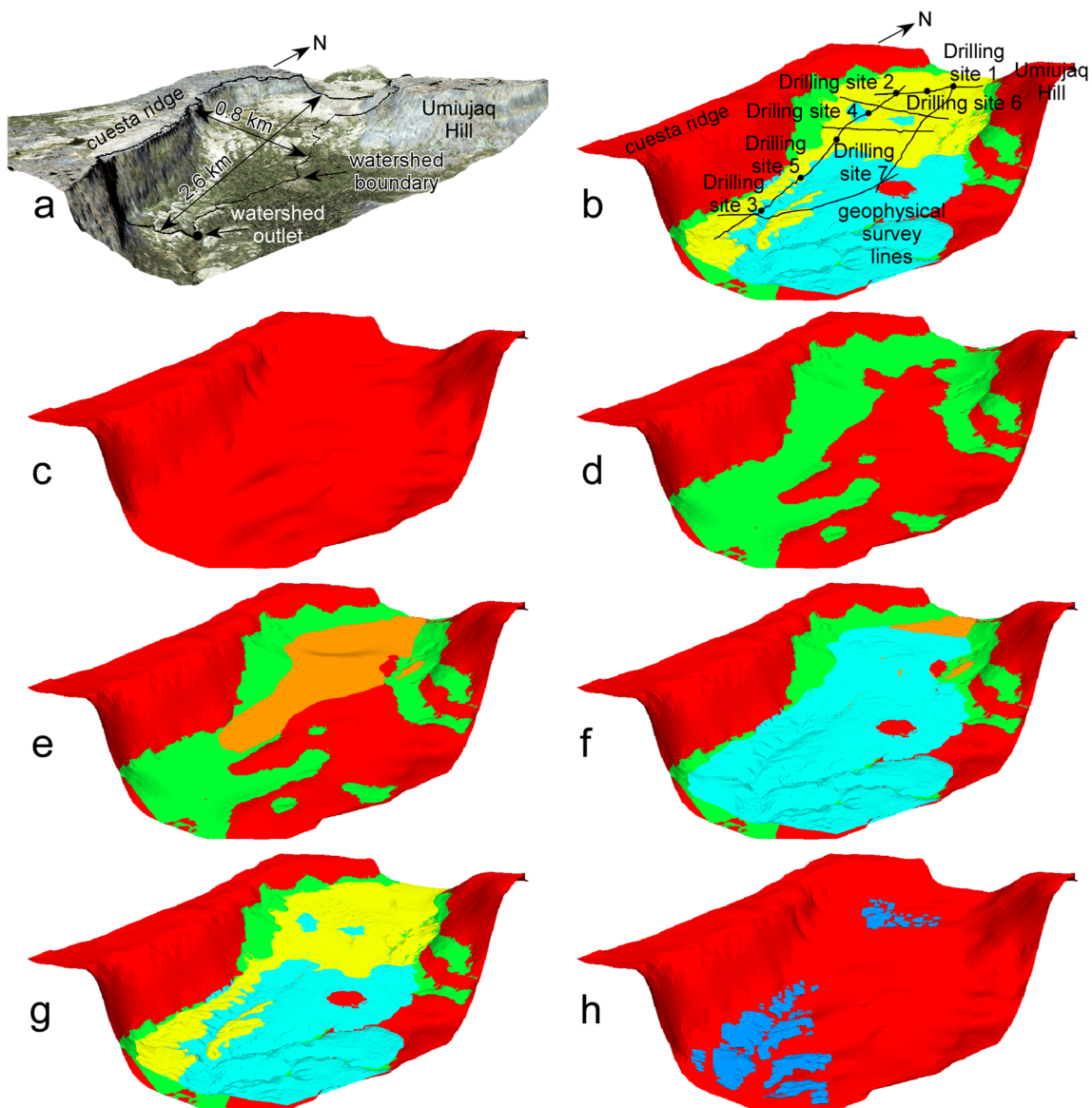


Fig. 9 Three-dimensional geological model of the studied watershed in the Tasiapik Valley: **a** IKONOS satellite image taken on July 27, 2005 of the Tasiapik Valley draped on a digital elevation model. The watershed boundary and outlet are also drawn in this view. **b** Full model along with the drilling sites and geophysical survey lines. **c** Undifferentiated bedrock

topography (unit R). **d** Undifferentiated gravelly sand (unit T). **e** Medium sand (unit Gs). **f** Silty sand (unit Ma). **g** Undifferentiated sand (unit M). **h** Floating extent of ice-rich permafrost (unit Pmf). Note the vertical exaggeration of 2:1

similar to a deltaic deposit as imaged by GPR profiling in the upper valley (Fig. 8). This unit can be as thick as 15 m uphill in the upper valley and disappears somewhere downhill between the drilling sites 6 and 2 (Fig. 3) where the water column was too high from strong tidal currents and transport of sand. As soon as this opening between the cuesta front and Umiujaq Hill in Tasiapik Valley closed around 6,875 cal years BP, the intertidal action stopped and the deposition of geofacies Mi was completed.

Littoral and pre-littoral sediments (geofacies Mb)

Following the progressive land emergence from 6,875 to 2,000 cal years BP, the surficial layer of sediments in the Tasiapik Valley were later reworked over a thickness of about 1 m through littoral action (geofacies Mb; Fig. 5). When the lower part of the watershed at an elevation of about 35 m emerged around 2,000 years BP, the littoral action stopped.

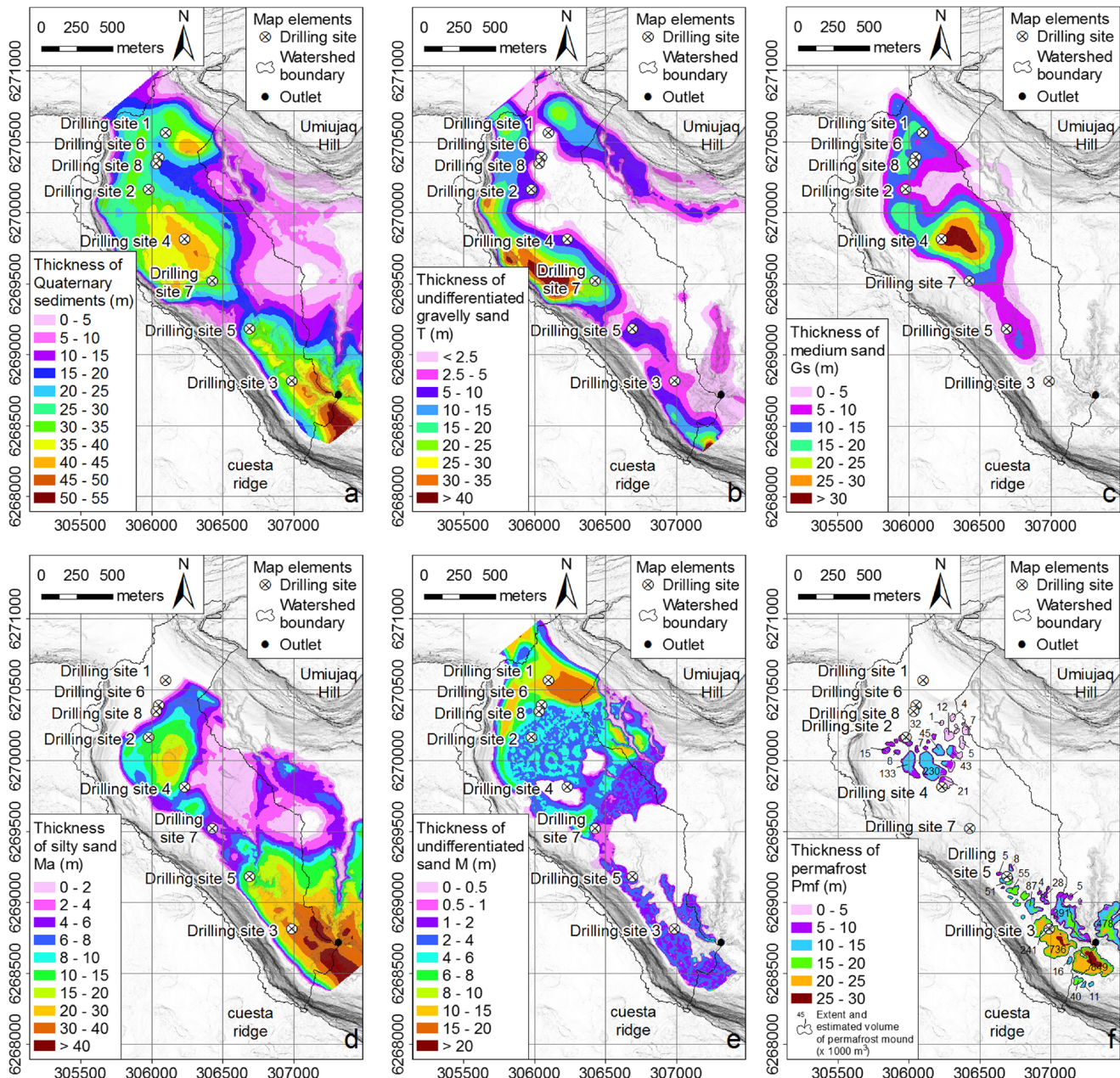


Fig. 10 Thickness of units in the Tasiapik Valley assessed from the 3D geological model of the watershed (Fig. 9): **a** undifferentiated Quaternary sediments; **b** undifferentiated gravelly sand (unit T); **c** medium sand (unit

Gs); **d** silty sand (unit Ma); **e** undifferentiated sand (unit M); **f** ice-rich permafrost (unit Pmf)

Alluvial sediments (geofacies A)

Recent sandy alluvial deposits underlie the small stream which drains the watershed into Tasiujaq Lake (geofacies A in Fig. 3c). Since the extent of this unit only becomes significant outside of the watershed close to its outlet, it is not considered in the local stratigraphy (Table 1). However, this small stream and other small springs from the upper aquifer (Lemieux et al. 2020, this issue) are eroding the Quaternary deposits in the Tasiapik Valley.

Permafrost aggradation and degradation

After the land emerged and came in contact with the cold climate, permafrost only began to aggrade in the Quaternary deposits of the Tasiapik Valley, around 2,000 cal years BP. Based on peat stratigraphy and radiocarbon dating in the area of Umiujaq, Allard et al. (1986) identified two cold periods from 1,500 to 1,050 cal years BP and from 650 to 200 cal years BP favorable for the aggradation of permafrost

along the east coast of Hudson Bay. Raised periglacial landforms due to the accumulation of segregation ice lenses in frost-susceptible marine silty sand (geofacies Ma; Fig. 4) under the form of ice-rich permafrost islets known as permafrost mounds are found in the Tasiapik Valley (Fig. 2). The thickness of segregation ice lenses can range from few millimeters to few centimeters (Fig. 4). The average volumetric ice content of ice-rich permafrost of these islets in the Tasiapik Valley can be in excess of 50% (Calmels and Allard 2008). The diameter of permafrost mounds can be as low as 20 m but as large as 300 m (Fig. 3c). The height of their top is few meters above their surroundings due to frost heaving (Fig. 2). A relationship exists between the permafrost thickness and diameter of permafrost mounds (Lévesque et al. 1988); the larger the diameter of the mounds, the deeper the permafrost is. Typical permafrost thickness in the Tasiapik Valley varies from about 4 m for small permafrost mounds to in excess of 25 m for permafrost plateau (Fig. 6b; El Baroudi and Fortier 2014; Fortier et al. 2008; Fortier and Yu 2012). The active layer, the surficial layer affected by freeze–thaw cycles, is from 1.5 to 2 m thick where the silty sand unit outcrops in the lower valley. In the upper part of the valley, some permafrost mounds have a sandy cover (geofacies Mb; Fig. 6b). In such case, the active layer thickness is in excess of 3 m. The depressions between the permafrost mounds are free of permafrost.

At the end of the Little Ice Age (LIA) around 1850, the climate in Nunavik was slightly colder by about 1 °C compared to the 1961–1990 reference period (Chouinard et al. 2007). This period corresponds to the maximum extent of permafrost in the area. The warming between the end of the LIA and the early 1900's somewhat faded during a period of slight cooling from 1940 to 1960 (Chouinard et al. 2007). A marked warming trend from 2 to 3 °C over the last 25 years has also been observed in Nunavik (Chouinard et al. 2007). Due to this climate warming, permafrost is currently degrading in the Tasiapik Valley and elsewhere in Nunavik (Fortier and Aubé-Maurice 2008). The complete thawing of permafrost mounds leaves ramparted thermokarst ponds (Fortier and Aubé-Maurice 2008).

Local stratigraphy

The changes in local stratigraphy from uphill to downhill in the valley, as shown in Figs. 5 and 6b, are closely related to the evolution of the physical processes of sedimentation and deposition of Quaternary sediments in the valley relative to the position of the ice front during LIS retreat, marine transgression of the postglacial Tyrrell Sea, changes in sea level and land emergence over time, and the valley topography and orientation. Gradual changes in the medium of disposition over time resulted in smooth transitions between the different geofacies observed in the Tasiapik Valley (Fig. 5; Table 1).

This is the reason why the stratigraphic contacts between these geofacies are not always sharp but rather progressive. For instance, several thin beds of sand were observed in samples of marine silty sand sediments (geofacies Ma) due to current traction in a still energetic depositional environment during meltwater outbursts at the retreating ice front away from the Tasiapik Valley (Fig. 4).

At each drilling site (Fig. 3), the Paleoproterozoic bedrock from the Richmond Gulf Group was sampled. The bedrock underlying the Tasiapik Valley is composed of hematized basalt of the Persillon Formation in the upper part of the valley (geofacies Ri in drilling sites 1, 6, 8, 2, 4 and 7; see Fig. 3 for the location of drilling sites) and arenite of the Pachi Formation (geofacies Rs in drilling sites 5 and 3) in the lower part of the valley (Figs. 5 and 6b). Based on the bedrock stratigraphy of the study area (Labbé and Lacoste 2004), these two rock formations of the Richmond Gulf Group are located below the subaerial basalt lava flows and sedimentary sequences of the Nastapoka Group which are visible along the cuesta escarpments (Fig. 2).

The thickness of Quaternary sediments in the valley varies between 21.5 m at drilling site 6 and 43 m at drilling site 4. In total, from top to bottom, based on their genesis, six geofacies of unconsolidated sediments were found in the Tasiapik Valley (Table 1): (1) littoral and pre-littoral sediments (geofacies Mb), (2) intertidal sediments (geofacies Mi), (3) offshore sediments (geofacies Ma), (4) subaqueous outwash sediments (geofacies Gs), (5) ice-contact sediments (geofacies GxT), and (6) till (geofacies T). The surficial littoral and pre-littoral sediments overlying the intertidal sediments was observed in shallow pits close to drilling sites 1 and 6 located in the upper valley. The geofacies Mi are made of sand beddings inclined toward the Tasiujaq Lake (Fig. 8). At these six geofacies, the ones of bedrock Ri and Rs can be added (Table 1).

As found from the piezometers installed in the watershed (Fig. 3a), two aquifers and an aquitard were identified within the watershed (Fig. 6b):

1. An upper aquifer in pre-littoral and littoral sediments (geofacies Mb) above offshore sediments (geofacies Ma)
2. A lower aquifer in glaciofluvial sediments and glacial sediments (geofacies Gs and T)
3. An aquitard in marine sediments (geofacies Ma) discontinuously invaded by ice-rich permafrost which partly confines the lower aquifer

Interpretative cryo-hydrogeological cross-sections from the geophysical investigation

The interpretative cryo-hydrogeological cross-section assessed from the models of electrical resistivity and

chargeability as a function of units (Table 1) along the geophysical survey lines L0 + 00 and TL4 + 00 is given in Fig. 6b (see Fig. 3b for the location of these survey lines). The stratigraphic contacts between the units and the hydraulic heads as observed in the piezometers few days after their installation in the boreholes in August 2012 (Fortier et al. 2017) are also provided in Fig. 6b.

To overcome the shortcomings of IPT in accurately identifying stratigraphic contacts, an objective interpretation method was developed in this study to extract quantitative information for the investigation of periglacial environments (Banville et al. 2016). This objective interpretation methodology is based on interface detection using the resistivity gradient criterion developed by Nguyen et al. (2005) and on an approach of forward/inverse modelling (FIM) of IPT driven by prior data from drilling logs (Fig. 5). This method was used to delineate the stratigraphic contacts between the units identified in Table 1.

The expected ranges of electrical resistivity (Fortier et al. 2008; Oldenborger and LeBlanc 2015) and chargeability (El Baroudi and Fortier 2014) for different types of soil can be used to discriminate the different units in the cryo-hydrogeological cross-section. For instance, the silty sand in unit Ma has electrical resistivity ranging from 100 Ω -m when unfrozen and saturated to in excess of 10,000 Ω -m for ice-rich frozen silty sand, while the boundary of 1,000 Ω -m separates unfrozen from frozen silty sand (Fortier et al. 2008). However, the values of electrical resistivity expected for ice-rich permafrost in silty sand are in the same range as those for dry sand; nevertheless, as mentioned earlier, there is a close link between the absence/presence of ice-rich permafrost as permafrost mounds scattered in the valley and raised landforms due to frost heave and accumulation of segregation ice lenses (Figs. 2, 3, and 4). The local topography with the topographic highs can be thus used to discriminate ice-rich permafrost mounds from deposits of dry sand. Moreover, dry sand has higher electrical chargeability than ice-rich ground (El Baroudi and Fortier 2014)—for instance, in the lower part of the valley, the zones of electrical resistivity above 10,000 Ω -m and low electrical chargeability less than 2 mV/V in the models of electrical resistivity and chargeability (Fig. 6a), respectively, associated to topographic highs are ice-rich permafrost mounds in the silty sand unit Ma. In contrast, in the upper part of the valley, the zones of high values of electrical resistivity and chargeability (Fig. 6a) in a flat zone are dry sand in unit M. Since the hematized basalt in the upper valley has very high electrical chargeability, the contact between the unconsolidated sediments and bedrock at depth was therefore easily delineated in this section of the survey line—for instance, the high values of electrical chargeability at depth in the model of electrical chargeability in Fig. 6a between the distance from 200 to 600 m and from 1,100 to 1,800 m are due to the hematized basalt. This interpretation was confirmed by short SRT surveys (results not shown herein; see Banville 2016) and the borehole

logs in drilling sites 1, 2, 4, and 7. These few interpretation keys together with the objective interpretation method (Banville et al. 2016) were used to produce the interpretative cryo-hydrogeological cross-section (Fig. 6b). This cross-section also takes into account the available geospatial information (Fig. 3) and stratigraphic logs (Fig. 5) to further constrain the interpretation of the electrical resistivity and chargeability models. Similar interpretative cryo-hydrogeological cross-sections as in Fig. 6b were produced from the models of electrical resistivity and chargeability along the other IPT survey lines (Fig. 7) but there are not shown herein.

The thick deposit of dry and partially frozen sand in the upper valley led to an exceptionally large depth of investigation for the GPR profile in excess of 35 m along the geophysical survey line L0 + 00 in the upper valley (Fig. 8; see Fig. 3b for the location of this survey line). However, the GPR was of little use in the lower valley since the depth of investigation was limited due to signal attenuation in the conductive unfrozen silts (geofacies Ma) and multiple diffractions in ice-rich permafrost which rapidly dampens the radar signal. The interpretative cross-section along with the stratigraphic logs at drilling sites 1 and 6 superimposed on the GPR profile is shown in Fig. 8. Sedimentary structures specific to each geofacies produce major differences in GPR signals in GPR profiles which can be used to delineate the stratigraphic contacts between geofacies. For instance, the reflectors associated to beddings of the intertidal sediments (geofacies Mi in Fig. 8) inclined to the south are visible in this GPR profile. The black lines in the GPR profile delineate the stratigraphic contacts between the geofacies (Fig. 8). This cross-section interpreted from the GPR profile along the geophysical survey line L0 + 00 (Fig. 8) can be directly compared to the first 500 m of the interpretative cryo-hydrogeological cross-section in Fig. 6b derived from the models of electrical resistivity and chargeability (Fig. 6a). The spatial coverage of the geophysical investigation in the Tasiapik Valley (Fig. 7) along with other available information was enough to constraint the 3D geological model of the watershed.

Three-dimensional geological model of the watershed

By applying the principle of parsimony, a comprehensive geological model should only contain a minimum number of units needed for a complete geological description of the watershed. The descriptive criteria used for each unit must therefore produce unique physical properties. Therefore, to decrease the complexity of the local stratigraphy and reduce the number of geofacies observed in the Tasiapik Valley (Table 1), the littoral and pre-littoral sediments (geofacies Mb) and intertidal sediments (geofacies Mi), and the till (geofacies T) and frontal moraines (geofacies GxT), are considered as two undifferentiated geofacies, respectively, and identified as two units in the

Table 2 Statistics on the area and volume of units within the watershed boundary in the Tasiapik Valley (see Figs. 9 and 10)

Unit (see Table 1)	Area (km ²)	Volume ($\times 10^6$ m ³)
Studied watershed	2.23 (100%)	na
Quaternary deposits	1.72 (76.9%)	47.3 (100%)
Undifferentiated sand M	1.11 (49.8%)	8.59 (18.1%)
Silty sand Ma	1.17 (52.5%)	15.3 (32.2%)
Medium sand Gs	0.90 (40.5%)	10.1 (21.4%)
Undifferentiated gravelly sand T	1.18 (53.1%)	13.4 (28.3%)
Ice-rich permafrost Pmf	0.24 (10.7%)	3.18 (6.7%)

3D geological model. Although their genesis is different, these pairs of geofacies have similar particle-size distribution not shown herein (see their effective diameter D_{10} corresponding to 10% finer in the particle-size distribution in Table 1) and material properties allowing their merging in units. Therefore, after merging these geofacies, six different units including ice-rich permafrost formed in the frost-susceptible silty sand unit and undifferentiated bedrock are part of the 3D geological model (Table 1).

The 3D geological model is shown in the form of the upper 3D surfaces of the units (Fig. 9) and the maps of unit thickness (Fig. 10) in the Tasiapik Valley. Statistics on the area and volume of units within the watershed boundary are also given in Table 2. This geological model provides exceptional insights into the local stratigraphic architecture and geometries of Quaternary deposits, stratigraphic relationship between the aquifers and aquitards, and extent of ice-rich permafrost within the Tasiapik Valley.

Aquifers in the 3D geological model

The two aquifers identified within the watershed are (Fig. 6b):

1. The upper aquifer in the undifferentiated sand unit M in Figs. 9g and 10e above the silty sand unit Ma in Figs. 9f and 10d
2. The lower aquifer in the medium sand unit Gs in Figs. 9e and 10c and in the undifferentiated gravelly sand unit T in Figs. 9d and 10b.

From the geometries of units and their stratigraphic relationships as illustrated in Figs. 9 and 10, in the upper reaches of the watershed, the recharge of the lower aquifer occurs where the silty sand unit Ma is absent (Figs. 9f and 10d). The lower aquifer is also recharged through water infiltration along the cuesta escarpment where the geofacies GxT outcrops (Fig. 3c; Lemieux et al. 2020, this issue). Groundwater in the lower aquifer flows downgradient within the layer of

glacial and glaciofluvial sediments (Figs. 9d,e and 10b,c) along the contact with the bedrock which acts as a low-permeability boundary (Fig. 9c).

Where there is no hydraulic connection between the surficial unit M and the units Gs and T at depth because they are separated by the unit Ma acting as an aquitard (Figs. 9f and 10d), groundwater accumulates in the unit M to form the upper aquifer. This aquifer begins close to drilling sites 6 and 8 (see the northwestern end of unit Ma in Figs. 10d and 6b) and ends close to drilling site 7 (see the southeastern end of unit M in Figs. 10e and 6b). Small streams and springs from this upper aquifer are found at the southeastern end of unit M (Lemieux et al. 2020, this issue).

Partly confining aquitard

The lower aquifer is partly confined by the layer of low-permeability silty sand (unit Ma) acting as an aquitard and discontinuously ice-rich permafrost formed in this layer of frost-susceptible material. The spatial extent of unit Ma relative to that of the units T and Gs can be appreciated by comparing Fig. 10d with Fig. 10b,c, respectively. The stratigraphic relationship with ice-rich permafrost is also shown in Fig. 10f. In the lower reaches of the Tasiapik Valley, unit Gs is absent (Figs. 6b, 9e, and 10c) and the lower aquifer is therefore restricted to the unit T (Figs. 9d and 10c). In the same area, the piezometric surface of the lower aquifer is located within the aquitard (Fig. 6b). Artesian conditions are sometimes observed in fall in piezometer Pz4 at drilling site 3 (Figs. 3a and 6b; Lemieux et al. 2020, this issue).

Permafrost

Discontinuous ice-rich permafrost formed in the unit Ma of frost-susceptible marine sediments (Figs. 9h and 10f). The permafrost mounds within the watershed occupy a total area of about 239,000 m², varying from 400 m² for the smallest permafrost mound to 39,800 m² for the largest, and representing about 10.7% of the watershed area or 20.4% relative to the area of geofacies Ma (Fig. 10f; Table 2). The permafrost volume within the watershed is roughly estimated at 3.2×10^6 m³ which represents a volume of ground ice of about 1.6×10^6 m³ considering an average volumetric ice content of 50%. Even if the permafrost completely degrades over the coming decades (as suggested in the numerical model of Dagenais et al. 2020, this issue), this disappearance would not affect the degree of confinement of the lower aquifer since the hydraulic properties of unit Ma would not significantly change due to permafrost degradation. However, meltwater released from permafrost degradation will recharge the lower aquifer and may modify the groundwater geochemistry (Cochand et al. 2020, this issue).

Discussion

Three-dimensional geological mapping directly fulfills the need for improved subsurface modelling of materials and structures to address several current geoscience issues (Thorleifson et al. 2010) such as studying hydrogeological context of degrading permafrost environment and dynamics of groundwater and permafrost in a changing climate (McClymont et al. 2013; McKenzie and Voss 2013; Walvoord et al. 2012). Even if the assessment of spatial extent of permafrost using airborne geophysical investigation is useful to assess the impacts of groundwater flow on permafrost dynamics at a regional scale (Minsley et al. 2012), the architecture and geometries of Quaternary deposits have also to be taken into account for understanding the hydrogeological context and groundwater dynamics (Légaré-Couture et al. 2018). In addition to a good knowledge of the Quaternary chronology and sedimentary (Légaré-Couture et al. 2018), ground-based geophysical investigation at a much lower cost than airborne geophysical investigation can provide the needed information not only on spatial extent of permafrost (McClymont et al. 2013) but also on Quaternary deposits (Pugin et al. 2013).

Development of the 3D geological model of the watershed

Knowledge of the Quaternary chronology and sedimentary, and periglacial processes taking place in the Tasiapik Valley at Umiujaq formed the basis for construction of the 3D geological model of the watershed. This knowledge comes in part from the mapping of Quaternary deposits by photo-interpretation and field validation, a high-resolution digital elevation model obtained from an airborne LiDAR survey, and drilling (Figs. 3 and 5).

Using a genetic approach and based on the mechanisms that explain the genesis of Quaternary deposits found in the Tasiapik Valley, six sedimentary geofacies were distinguished from the youngest to the oldest (Table 1): (1) the littoral and pre-littoral geofacies Mb, (2) the intertidal geofacies Mi, (3) the offshore geofacies Ma, (4) the subaqueous outwash geofacies Gs, (5) the ice-contact geofacies GxT, and (6) the till T. Ice-rich permafrost formed in the offshore sediments (geofacies Ma) is considered as the cryofacies Pmf (Table 1). Even if their genesis is different, the geofacies Mi and Mb, and the geofacies T and GxT have similar grain size composition. These geofacies could be merged based on their similar physical, hydrogeological, and geophysical properties. These geofacies overly the bedrock which is composed of hematized basalt in the upper reaches of the valley, geofacies Ri, and arenite in the lower part of the valley, geofacies Rs (Figs. 5 and 6b; Table 1).

To reduce the complexity of the stratigraphy in the Tasiapik valley, based on the types of materials and their physical properties, the observed geofacies were reduced to six units (Table 1): (1) the ice-rich permafrost unit Pmf in the silty sand unit Ma, (2) the undifferentiated sand M (merged geofacies Mi and Mb), (3) the silty sand unit Ma, (4) the medium sand Gs, (5) the undifferentiated gravelly sand T (merged geofacies GxT and T), and (6) the undifferentiated bedrock R (merged geofacies Ri and Rs). These units are part of the 3D geological model of the studied watershed.

The geophysical investigation carried out in the study site was mainly based on IPT and GPR profiling. From the models of electrical resistivity and chargeability developed from the inversion of the induced polarization data, the geoelectrical structures in the soils can be imaged along the geophysical survey lines. Knowing their specific ranges of electrical properties, these models can be interpreted in terms of units (Table 1). Since these geofacies Mi and Mb are composed of sands of similar grain-size distribution, they cannot be distinguished by their electrical resistivity or their hydrogeological properties. These geofacies were therefore undifferentiated and merged as the unit M in the interpretative cryo-hydrogeological cross-section (Fig. 6b) and 3D geological model (Figs. 9 and 10). In contrast, the unit M and Ma can be distinguished by their ranges of electrical resistivity. At depth, however, the electrical resistivity contrasts between the units Gs and T cannot be resolved. Rather, these units show a continuum of electrical resistivity due to the gradual evolution of the deposition medium that explains their genesis. In the upper reaches of the valley, the GPR profile has an exceptional depth of investigation due to a thick layer of resistive sands and gravels which allows imaging the sedimentary structures of geofacies Mb, Mi, Gs, and GxT from the surface down to the bedrock contact. This GPR profile improved the interpretation of the models of electrical resistivity and chargeability. The mapping of ice-rich permafrost mounds (cryofacies Pmf) was based not only on their signature on the models of electrical resistivity and chargeability but also on the topographic highs scattered through the valley floor due to frost heave (Figs. 2 and 3). A geophysical investigation of the entire watershed was not possible with the available technical resources and research funding, and due to the limited time allotted to this study; however, the spatial coverage of the geophysical survey lines is considered enough for the construction of the 3D geological model.

Constraints for the 3D geological model were based on numerous sources including knowledge of the sedimentary processes, Quaternary history and periglacial processes, the mapping of Quaternary deposits, the high-resolution digital elevation model, information from piezometers used for monitoring groundwater dynamics, as well as the objective interpretation of geophysical data leading to meaningful interpretative cryo-hydrogeological cross-

sections. The development of this model in GoCAD using a method of discrete smooth interpolation was completed in two steps. A first preliminary model was built from the available constraints. In the second step, synthetic cryo-hydrogeological cross-sections along the geophysical survey lines were created by analysing this preliminary model. These synthetic cross-sections were then compared to the interpretative ones derived from the geophysical investigation. Modifications were then made to the model based on these comparisons.

Model uncertainties

The 3D geological model has several sources of uncertainty which are mainly related to the density and quality of available information. In increasing order of importance, four main model uncertainties for the distribution of undifferentiated gravelly sand unit T, undifferentiated sand M, permafrost distribution, and bedrock topography have been identified.

Distribution of undifferentiated gravelly sand unit T

The geophysical methods used in this study to perform the geophysical investigation of the Tasiapik Valley have several intrinsic limitations such as their resolution, limited contrast between geofacies, and spatial coverage. Based only on the electrical resistivity and chargeability measured along the survey lines of induced polarization tomography (Figs. 3b, 6, and 7), it was impossible to distinguish the units T, Gs, and M. It was only possible to distinguish between the geofacies R, GxT, Gs, Mi, and Mb in the GRP profile (Fig. 8) based on their characteristic sedimentary structures in the upper reaches of the Tasiapik Valley where there is a thick succession of coarse-grained materials with an exceptionally large depth of investigation for GPR. Further down the valley, the GPR cannot detect the deep units Gs and T since the unit Ma becomes too thick and its high electrical conductivity attenuates the GPR signal. The scarce information on the distribution of these units is therefore limited to the surface mapping and drilling information. The method used to generate the units Gs and T in the 3D geological model allows a realistic representation but it may not be representative of the real distribution of these units. This may have a major impact on the hydrogeological simulations since it is a layer of high hydraulic permeability at the bottom of the model and constitutes a good aquifer in the valley. The sensitivity of hydrogeological simulations to the thickness of this layer should be studied since its influence on groundwater flow can be significant.

Distribution of undifferentiated sand M

Uncertainty in the distribution of unit M is also large because of limitations of the applied geophysical methods. Due to the

chosen electrode geometry for IPT, the geological contacts located at depths of less than about 10 m could not be resolved. Only the GPR provides enough resolution to resolve the geofacies Mb and Mi (Fig. 8). Since the GPR surveys were mainly restricted to the upper reaches of the valley, the information on the thickness of unit M is very scarce in the lower part of the valley. Following the mapping of Quaternary deposits (Fig. 3c), the thickness of this unit was estimated based on the map of Quaternary deposits (Fig. 3c). For the hydrogeological simulations, the level of details in the 3D geological model is not enough to allow an adequate characterization of the upper aquifer in this unit. The sensitivity of the hydrogeological simulations to the thickness of this layer should be studied since its influence on infiltration and surface runoff may be important.

Permafrost distribution

Since the hydrogeological simulations are intended to predict the evolution of groundwater dynamics under different scenarios of climate change (Dagenais et al. 2020, this issue), the permafrost distribution and characteristics in the Tasiapik Valley are important parameters to consider. As already mentioned, there is a close link between the topographic highs in the valley bottom and ice-rich permafrost (Fig. 2). Using stereoscopy of aerial photographs and a high-resolution digital elevation model (Fig. 3a,b), the extent of permafrost mounds as raised periglacial landforms was mapped throughout the valley with high accuracy (Fig. 3c). The uncertainty in the estimate of permafrost thickness at each permafrost mound is significant and probably greater than 20% away from the geophysical survey lines. Moreover, the 3D geological model does not provide any information on the distribution of ice content in ice-rich permafrost and from one permafrost mound to another.

Bedrock topography

The topography of bedrock can have a significant influence on hydrogeological simulations since it would act as a very low-permeability boundary since it is largely unfractured below the lower aquifer. As part of the data interpolation, strict smoothing constraints were applied to the bedrock topography to avoid random oscillations in GoCAD outside of the geophysical coverage area. Judging by the topographic variability of the rock outcrops in the Umiujaq region, the topography of bedrock below the Quaternary sediments of the Tasiapik Valley is most likely more irregular than that suggested by the 3D model.

In summary, the 3D geological model of the Tasiapik Valley presented herein is considered representative of the real geological system at a scale of about 100 m laterally

for the unit extent and 10 m vertically for the contacts between thick units at depth away from the geophysical survey lines. The density of available observations was not enough to finely reproduce the system. Hydrogeological simulations based on this 3D geological model must take into account this model uncertainty.

Conclusions

In cold regions, it is critical to understand the dynamics of permafrost and groundwater in the context of climate change for the sustainable use of natural resources such as groundwater. Thermo-hydraulic numerical modelling of periglacial and hydrogeological processes is required to accurately simulate the evolution of groundwater systems in degrading permafrost environment due to climate change. The accuracy of numerical modelling depends not only on the development of numerical codes of these fully coupled nonlinear processes but also on realistic conceptual model of degrading permafrost environment. These processes are strongly influenced by the architecture and geometries of Quaternary deposits and the spatial extent of permafrost. Details about permafrost environment are often lacking because of the difficulty in probing the subsurface. Typically, inferences about Quaternary deposits and permafrost distribution are largely based on conceptual models derived from surface observations, sparse boreholes, and limited geophysical data. Realistic models of permafrost environment are needed to improve the meaningfulness of numerical modelling of periglacial and hydrogeological processes.

The main objective of the study presented herein was to build a realistic 3D geological model of a small watershed located in a valley in the discontinuous permafrost zone near the Inuit community of Umiujaq along the east coast of Hudson Bay, Nunavik (Québec), Canada. The construction of this model was based on the results of a thorough geomorphological, geotechnical, hydrogeological, and geophysical investigation of the study site. All available data on the Quaternary deposits and permafrost distribution in the watershed were integrated into GoCAD to build the 3D geological model. This model was used to assess the hydraulic budget and groundwater geochemistry in the watershed, to develop a numerical model of coupled groundwater flow and heat transfer at the scale of permafrost mounds, and to understand the groundwater flow dynamics and permafrost evolution in the watershed affected by climate change (see companion papers in this topical collection of *Hydrogeology Journal*).

The valley bottom is covered by up to 43 m of glacial, glaciofluvial, and marine sediments overlying the bedrock. Degrading permafrost mounds are found in a deposit of frost-susceptible sandy-silt and silty-sand and occupy about 10.7% of the watershed area. Two aquifers were identified in the watershed: an upper aquifer in surficial sandy sediments

and a lower aquifer in glacial and glaciofluvial sediments. The upper aquifer is located in the middle of the valley where the intertidal, littoral, and pre-littoral sediments cover the fine-grained marine sediments. The lower aquifer is unconfined in the upper reaches of the valley but becomes confined by offshore sediments invaded by permafrost in the lower part of the valley.

Based on observations from boreholes, natural stratigraphic sections and interpretive results from the various geophysical surveys, the stratigraphic contacts between the sedimentary units could not be clearly defined, but were rather gradual. Although the proposed 3D geological model presents units separated by sharp stratigraphic contacts, the genetic interpretation of the sedimentary units suggests rather gradual transitions of hydraulic and thermal properties between these units. Because of the limited density of the available observations and the assumptions used to build the model, the representativeness of the model is considered limited to a scale of about 100 m laterally and 10 m vertically for the contacts between thick facies at depths and away from the geophysical survey lines.

The integrated approach presented herein to delineate the cryo-hydrogeological context of a watershed in a degrading permafrost environment in Nunavik, Canada, can be used to identify groundwater resources in similar periglacial environments. The 3D geological model developed in this study was used as a basis for quantifying groundwater exploitation potential along with evaluating aquifer sustainability in cold environments. New knowledge and expertise were developed in cold regions hydrogeology for the sustainable use of groundwater in cold regions as a source of drinking water. The likely increase in groundwater availability due to the permafrost degradation as a positive impact of climate change is a unique opportunity to use this natural resource for supplying drinking water to northern communities in degrading permafrost environments.

Acknowledgements A preliminary and condensed version of this paper was previously published in the Proceedings of the 70th Canadian Geotechnical Conference, Ottawa, Ontario, Canada (Fortier et al. 2016). The authors of this publication retain the copyright.

Thanks are due to the editor and associate editor of *Hydrogeology Journal*, and three anonymous reviewers for their comments, which significantly improved the final version of this paper. We would like to express our sincere gratitude to the Inuit community of Umiujaq for their hospitality and friendly support, and for providing access to their land. Thanks are also due to G. Auger, L. Beaupré, M. Cochand, M. El Baroudi, J. Leblanc, P. Lamontagne-Hallé, M. Mayers, R. Murray, J. Sottas, and M.-C. Talbot Poulin for their help in the field. The piezometers in the Tasiapik Valley were installed by G. Chapdelaine, C. Raymond, and S. Prescott from the drilling company Gestion Chapdelaine inc. The involvement of S. Moore, L. Ricard, R. Lacouline, and D. Myrand from the Ministère de l'Environnement et de la Lutte contre les changements climatiques of Québec and the logistical support from the Centre d'études nordiques are gratefully acknowledged. The help of Olivier Rabeau was instrumental in using GoCAD. The research presented herein was supported by the Ministère de l'Environnement et de la Lutte contre les changements climatiques of

Québec and the Natural Sciences and Engineering Research Council of Canada (via a Strategic Grant to R. Therrien, R. Fortier, J.-M. Lemieux, and J. Molson).

References

- Albers BMC, Molson JW, Bense VF (2020) Parameter sensitivity analysis of a two-dimensional cryo-hydrogeological numerical model of degrading permafrost near Umiujaq (Nunavik, Canada). *Hydrogeol J*. <https://doi.org/10.1007/s10040-020-02112-2>
- Allard M, Seguin MK (1985) La déglaciation d'une partie du versant Hudsonien des rivières Nastapoka, Sheldrake et à l'Eau Claire [Deglaciation of a portion of the Hudsonian side of the Nastapoka, Sheldrake and Eau Claire rivers]. *Géog Phys Quatern* 39:13–24
- Allard M, Seguin MK (1987) The Holocene evolution of permafrost near the tree line, on the eastern coast of Hudson Bay (northern Quebec). *Can J Earth Sci* 24(11):2206–2222. <https://doi.org/10.1139/e87-209>
- Allard M, Seguin MK, Lévesque R (1986) Palsas and mineral permafrost mounds in northern Québec, international geomorphology, part II. In: Gardiner V (ed) 1st International Conference on Geomorphology. Wiley, London, pp 285–309
- Banville DR (2016) Modélisation cryohydrogéologique tridimensionnelle d'un bassin versant pergélisolé: une étude cryohydrogéophysique de proche surface en zone de pergélisol discontinu à Umiujaq au Québec nordique [Three-dimensional cryohydrogeological modeling of a permafrost watershed: a near-surface cryohydrogeophysical study in the discontinuous permafrost zone at Umiujaq in northern Quebec]. MSc Thesis, Université Laval, Québec City, QC, 278 pp
- Banville DR, Fortier R, Dupuis C (2016) Objective interpretation of induced polarization tomography using a quantitative approach for the investigation of periglacial environments. *J Appl Geophys* 130: 218–233. <https://doi.org/10.1016/j.jappgeo.2016.04.019>
- Buteau S, Fortier R, Allard M (2005) Rate-controlled cone penetration tests in permafrost. *Can Geotech J* 42:184–197
- Calmels F, Allard M (2008) Segregated ice structures in various heaved permafrost landforms through CT scan. *Earth Surf Process Landform* 33:209–225. <https://doi.org/10.1002/esp.1538>
- Chandler FW (1988) The early Proterozoic Richmond Gulf graben, east coast of Hudson Bay, Quebec. *Geol Surv Can Bull* 362:76
- Chouinard C, Fortier R, Mareschal JC (2007) Recent climate variations in the subarctic inferred from three borehole temperature profiles in northern Quebec Canada. *Earth Planet Sci Lett* 263:355–369. <https://doi.org/10.1016/j.epsl.2007.09.017>
- Cochand M, Molson JW, Barth JAC, van Geldern R, Lemieux JM, Fortier R, Therrien R (2020) Rapid groundwater recharge dynamics determined from hydrogeochemical and isotope data in a small permafrost watershed near Umiujaq (Nunavik, Canada). *Hydrogeol J*. <https://doi.org/10.1007/s10040-020-02109-x>
- Dagenais S, Molson JW, Lemieux JM, Fortier R, Therrien R (2020) Coupled cryo-hydrogeological modelling of permafrost dynamics near Umiujaq (Nunavik, Canada). *Hydrogeol J*. <https://doi.org/10.1007/s10040-020-02111-3>
- De Pascale GP, Pollard WH, Williams KK (2008) Geophysical mapping of ground ice using a combination of capacitive coupled resistivity and ground-penetrating radar, Northwest Territories, Canada. *J Geophys Res Earth Surf* 113(F2):F02S90
- El Baroudi M, Fortier R (2014) Tomographie bidimensionnelle et tridimensionnelle de polarisation provoquée d'un pergélisol riche en glace au Québec nordique, Canada [Two- and three-dimensional induced polarization tomography of ice-rich permafrost in northern Quebec, Canada]. *Notes Mém Serv Géol Maroc* 557: 107–124
- Eyles CH, Eyles N, Miall AD (1985) Models of glaciomarine sedimentation and their application to the interpretation of ancient glacial sequences. *Palaeogeogr Palaeoclimatol Palaeoecol* 51(1–4):15–84. [https://doi.org/10.1016/0031-0182\(85\)90080-X](https://doi.org/10.1016/0031-0182(85)90080-X)
- Fortier R, Aubé-Maurice B (2008) Fast permafrost degradation near Umiujaq in Nunavik (Canada) since 1957 assessed from time-lapse aerial and satellite photographs. Proceedings, 9th International Conference on Permafrost, Fairbanks, AK, June 29–July 3, 2008, pp 457–462
- Fortier R, Yu W (2012) Penetration rate-controlled electrical resistivity and temperature piezocone penetration tests in warm ice-rich permafrost in northern Quebec (Canada). Proceedings, 15th International Specialty Conference on Cold Regions Engineering, Québec City, August, 2012, 11 pp
- Fortier R, LeBlanc AM, Buteau S, Allard M, Calmels F (2008) Internal structure and conditions of permafrost mounds at Umiujaq in Nunavik, Canada, inferred from field investigation and electrical resistivity tomography. *Can J Earth Sci* 45:367–387
- Fortier R, Banville DR, Lemieux JM, Ouellet M, Therrien R (2016) Geophysical investigation of aquifers in a degrading permafrost environment in northern Quebec, Canada. Proceedings, 11th International Conference on Permafrost, Potsdam, Germany, June 2016, 2 pp
- Fortier R, Lemieux JM, Molson JW, Therrien R, Cochand M (2017) Rapport de synthèse sur le déploiement du réseau Immatsiak à Umiujaq au Québec nordique pour le suivi des eaux souterraines en régions froides [Synthesis report on the deployment of the Immatsiak network at Umiujaq in northern Quebec for groundwater monitoring in cold regions]. Report, Ministère du développement durable, de l'Environnement et de la Lutte contre les changements climatiques du Québec, QC, 303 pp
- Government of Québec (2019) Réseau de suivi des eaux souterraines du Québec [Quebec Groundwater Monitoring Network]. Ministère de l'Environnement et de la Lutte contre les changements climatiques. <http://www.environnement.gouv.qc.ca/eau/piezo/index.htm>. Accessed December 21, 2019
- Grenier C, Anbergen H, Bense V, Chanzy Q, Coon E, Collier N, Costard F, Ferry M, Frampton A, Frederick J, Holmen J, Jost A, Kokh S, Kurylyk B, McKenzie J, Molson J, Mouche E, Orgogozo L, Pannetier R, Rivière A, Roux N, Rühaak W, Scheidegger J, Selroos J-O, Therrien R, Vidstrand P, Voss C (2018) Groundwater flow and heat transport for systems undergoing freeze-thaw: inter-comparison of numerical simulators for 2D test cases. *Adv Water Resour* 114:196–218. <https://doi.org/10.1016/j.advwatres.2018.02.001>
- Ireson AM, Van Der Kamp G, Ferguson G, Nachshon U, Wheeler HS (2013) Hydrogeological processes in seasonally frozen northern latitudes: understanding, gaps and challenges. *Hydrogeol J* 21(1):53–66
- Jamin P, Cochand M, Dagenais S, Lemieux JM, Fortier R, Molson JW, Brouyère S, (2020) Direct measurement of groundwater flux in aquifers within the discontinuous permafrost zone: an application of the finite volume point dilution method near Umiujaq (Nunavik, Canada). *Hydrogeol J*. <https://doi.org/10.1007/s10040-020-02108-y>
- KRG (2007) Lacs-Guillaume-Delisle-et-à-l'Eau-Claire Park Project. Status report, Kativik Regional Government, Renewable Resources, Environmental and Land Use Planning Department, Parks Section, Kuujuaq, QC, pp 257
- Labbé JY, Lacoste P (2004) Minéralisation en Cu-Ag dans les basaltes protérozoïques de la région du lac Guillaume-Delisle, Nouveau-Québec (Cu-Ag mineralization in Proterozoic basalts in the Lac Guillaume-Delisle area, northern Quebec). Report ET 2004–02, Ministère des Ressources naturelles, de la Faune et des Parcs du Québec, Québec City, QC, 32 pp
- Lavoie C, Allard M, Duhamel D (2012) Deglaciation landforms and C-14 chronology of the lac Guillaume-Delisle area, eastern Hudson Bay:

- a report on field evidence. *Geomorphology* 159–160:142–155. <https://doi.org/10.1016/j.geomorph.2012.03.015>
- LeBlanc AM, Fortier R, Allard M, Cosma CG (2004) Seismic cone penetration test and seismic tomography in permafrost. *Can Geotech J* 41:796–813
- LeBlanc AM, Fortier R, Cosma CG, Allard M (2006) Tomographic imaging of permafrost using a three-component seismic cone penetration test. *Geophysics* 71(5):H55–H65
- Lemieux JM, Fortier R, Talbot Poulin MC, Molson J, Therrien R, Ouellet M, Banville DR, Cochand M, Murray R (2016) Groundwater occurrence in cold environments: examples from Nunavik, Canada. *Hydrogeol J* 24(6):1–17. <https://doi.org/10.1007/s10040-016-1411-1>
- Légaré-Couture G, Leblanc Y, Parent M, Lacasse K, Campeau S (2018) Three-dimensional hydrostratigraphical modelling of the regional aquifer system of the St. Maurice Delta complex (St. Lawrence Lowlands, Canada). *Can Water Resour J* 43(2):92–112
- Lemieux JM, Fortier R, Murray R, Dagenais S, Cochand M, Delottier H, Therrien R, Molson JW, Pryet A, Parhizkar M (2020) Groundwater dynamics within a watershed in the discontinuous permafrost zone near Umiujaq (Nunavik, Canada). *Hydrogeol J*. <https://doi.org/10.1007/s10040-020-02110-4>
- Lévesque R, Allard M, Seguin MK (1988) Le pergélisol dans les formations quaternaires de la région des rivières Nastapoca et Sheldrake, Québec Nordique [Permafrost in the Quaternary formations of the Nastapoca and Sheldrake River area, northern Quebec]. Collection Nordica no. 51, Centre d'études nordiques, Université Laval, Québec City, QC, 23 pp
- Loke MH (2004) Tutorial: 2-D and 3-D electrical imaging surveys. Geotomo Software, Penang, Malaysia, 136 pp
- Lønne I (1995) Sedimentary facies and depositional architecture of ice-contact glaciomarine systems. *Sediment Geol* 98:13–43. [https://doi.org/10.1016/0037-0738\(95\)00025-4](https://doi.org/10.1016/0037-0738(95)00025-4)
- Mallet JL (1992) Discrete smooth interpolation in geometric modelling. *Comput Aided Des* 24:178–191. [https://doi.org/10.1016/0010-4485\(92\)90054-E](https://doi.org/10.1016/0010-4485(92)90054-E)
- McClymont AF, Hayashi M, Bentley LR, Christensen BS (2013) Geophysical imaging and thermal modeling of subsurface morphology and thaw evolution of discontinuous permafrost. *J Geophys Res Earth Surf* 118(3):1826–1837
- Michel FA, van Everdingen RO (1994) Changes in hydrogeologic regimes in permafrost regions due to climatic change. *Permafrost Periglac Process* 5(3):191–195. <https://doi.org/10.1002/ppp.3430050308>
- Minsley BJ, Abraham JD, Smith BD, Cannia JC, Voss CI, Jorgenson MT, Walvoord MA, Wylie BK, Anderson L, Ball LB, Deszcz-Pan TP, Wellman TP, Ager TA (2012) Airborne electromagnetic imaging of discontinuous permafrost. *Geophys Res Lett* 39(2)
- McKenzie JM, Voss CI (2013) Permafrost thaw in a nested groundwater-flow system. *Hydrogeol J* 21:299–316. <https://doi.org/10.1007/s10040-012-0942-3>
- Nguyen F, Garambois S, Jongmans D, Pirard E, Loke MHH (2005) Image processing of 2D resistivity data for imaging faults. *J Appl Geophys* 57:260–277. <https://doi.org/10.1016/j.jappgeo.2005.02.001>
- Oldenborger GA, LeBlanc AM (2015) Geophysical characterization of permafrost terrain at Iqaluit international airport, Nunavut, J Appl Geophys 123:36–49. <https://doi.org/10.1016/j.jappgeo.2015.09.016>
- Parent M, Paradis SJ, Boivin R. (2010) Formations superficielles: légende et notes descriptives—1/ 50 000 à 1/ 125 000, version 11 [Surficial formations: legend and descriptive notes—1:50,000 to 1:125,000, version 11]. Geological Survey of Canada, Québec Division, 10 pp
- Parhizkar M, Therrien R, Lemieux JM, Molson JW, Fortier R, Talbot-Poulin MC, Therrien P (2017) An integrated surface-subsurface flow model of the thermo-hydrological behavior and effect of climate change in a cold-region catchment in northern Quebec, Canada. Proceedings, GEOOttawa 2017, Ottawa
- Poly-Géo Inc. (2011) Surficial deposits and landforms in the region of Umiujaq, Nunavik. Map 1:10 000, Poly-Géo, Saint-Lambert, QC
- Poly-Géo Inc. (2014) Cartographie des matériaux de surface, chronologie de la déglaciation et stratigraphie des dépôts dans la Vallée-des-Trois à Umiujaq, Nunavik [Surficial mapping, deglaciation chronology, and stratigraphy of deposits in the Vallée-des-Trois at Umiujaq, Nunavik]. Report presented to Laval University, Poly-Géo, Saint-Lambert, QC, 26 pp and 2 maps
- Pugin AJM, Pullan SE, Duchesne MJ (2013) Regional hydrostratigraphy and insights into fluid flow through a clay aquitard from shallow seismic reflection data. *Lead Edge* 32(7):742–748
- Ross M, Parent M, Lefebvre R (2005) 3D geologic framework models for regional hydrogeology and land-use management: a case study from a Quaternary basin of southwestern Quebec, Canada. *Hydrogeol J* 13(5–6):690–707
- Thorleifson LH, Berg RC, Russell HA (2010) Geological mapping goes 3-D in response to societal needs. *GSA Today* 20(8):27–29
- Walvoord MA, Voss CI, Wellman TP (2012) Influence of permafrost distribution on groundwater flow in the context of climate-driven permafrost thaw: example from Yukon Flats Basin, Alaska, United States. *Water Resour Res* 48:W07524. <https://doi.org/10.1029/2011WR011595>